

## The Plasma Environment of Prominences – SOHO Observations

D. Moses, C.M. Korendyke, N. Moulton<sup>1</sup>

*Naval Research Laboratory, Code 7660.1, Washington, DC 20375, USA*

J. Newmark

*NASA/Goddard Space Flight Center, Greenbelt, MD 20771, USA*

**Abstract.** We describe the observational capabilities of the SOHO EIT and LASCO instruments for prominence research. A detailed comparison of EIT He II  $\lambda 304$  and BBSO H $\alpha$  images of a quiescent prominence reveals differences in fine scale structure which are attributed to differences in radiation emission and transport mechanisms. Absorption features present in coronal EIT images are attributed to dense prominence features located between the source of the coronal emission and the observer. These features provide the locations of prominence material in coronal image sequences. Observations of a prominence eruption in both EIT He II and LASCO C1 Fe XIV images show the heating of chromospheric material to coronal temperatures during the prominence eruption. In the last phase of the prominence eruption, a coronal mass ejection (CME) is initiated as a dark cavity forms over the prominence material and a bright loop-like structure forms over the dark cavity.

### 1. Introduction: The EIT and LASCO Instruments

Since the commissioning of the Solar and Heliospheric Observatory (SOHO) spacecraft in early 1996, the EUV Imaging Telescope (EIT) and the Large Angle Spectrometric Coronagraph (LASCO) have obtained new observations of prominences and prominence-associated phenomena. EIT images the Sun over a  $45 \times 45$  arcmin field of view in four EUV passbands: Fe IX,X at 171 Å, Fe XII at 195 Å, Fe XV at 284 Å, and He II at 304 Å. Emission in the Fe lines is from coronal plasma at characteristic temperatures of 1.3 MK, 1.6 MK, and 2.0 MK, respectively. Emission in the He II passband is from transition region plasma with a characteristic temperature of  $5.0 \times 10^4$  K. LASCO images provide coverage of the corona over a spatial range of 1.1 to 30  $R_{\odot}$  with three overlapping coronagraphs: C1 (1.1–3  $R_{\odot}$ ); C2 (2–6  $R_{\odot}$ ); C3 (4–30  $R_{\odot}$ ). The detector area is  $1024 \times 1024$  pixels for both the EIT and LASCO instruments.

---

<sup>1</sup>Allied Signal Technical Services Corp., Camp Springs, MD, USA

## 2. EIT He II 304 Å Observations

The EIT HeII imaging with a CCD detector improves the dynamic range of images by two orders of magnitude over previous HeII film imagery of the NRL slitless spectrograph on Skylab (Tousey et al. 1977). Sounding rocket observations by the NASA/GSFC SERTS instrument (e.g., Jordan et al. 1993) have added significantly to the study of HeII  $\lambda$ 304. However, suborbital observations of the Sun in HeII provide only a short sampling of highly varied and dynamic phenomena. The Lagrangian (L1) orbit of SOHO allows continuous imaging of the Sun, and the image cadence is limited primarily by the telemetry allocation. The highest sustained cadence of full disk, full resolution ( $1024 \times 1024$ ) HeII images was obtained for 23 hours beginning 22:00 UT on March 18, 1997 at the rate of 9 per hour. A movie of this sequence can be viewed at <http://lasco-www.nrl.navy.mil/iau/movie.html>.

The EIT HeII 304 Å bandpass width is 21 Å FWHM (Delaboudinière et al. 1995) and the only other line contributing significant power is the coronal Si XI 303.3 Å line. In the quiet Sun, the HeII line intensity dominates on the disk, while the Si XI line intensity becomes greater than the HeII intensity at heights  $> 20$  arcsec above the limb (Thomas 1994).

The emission mechanism for HeII is difficult to determine. Within the range of plasma conditions observed, collisional excitation, photoionization-recombination, radiative excitation, and resonant scattering can all be significant processes. A calculation including only collisional excitation using the CHIANTI procedures (Dere et al. 1997a) gives an emission measure of  $2.2 \times 10^{27} \text{ cm}^{-5}$  for the average quiet Sun EIT count rate, while the value obtained from a number of other transition region lines is of the order of  $2.8 \times 10^{26} \text{ cm}^{-5}$  (e.g., Dere and Mason 1993). This underestimate of the intensity of the HeII solar emission has been long appreciated and has led to the exploration of alternative emission mechanisms (e.g., Jordan 1975, Zirin 1975, Laming and Feldman 1992). The difference between emission mechanisms on the disk and in prominences is an additional complication. Further diagnostics such as spectroscopy of the HeII Balmer series (Laming and Feldman 1992), or filtergrams of another line of the HeII Lyman series may help to specify the processes involved in solar HeII emission.

A comparison of EIT HeII and BBSO  $H\alpha$  images of a quiescent prominence on March 9, 1997 is illustrated in Figure 1. The  $H\alpha$  image was obtained at the Big Bear Solar Observatory by H. Zirin using the high resolution OSL CCD camera. It is immediately apparent that the contrast between disk and prominence is less for HeII, allowing a wider dynamic range in the prominence. The outline of the prominence is well matched in the HeII and  $H\alpha$  images, while the detailed structure visible in the two images is not. These differences are consistent with the description of quiescent prominence HeII line emission by Laming and Feldman (1993), where photoionization and photoexcitation by coronal radiation are important processes. While the  $H\alpha$  structures appear to be excited by the chromospheric radiation below the prominence, the HeII structures appear to be excited by coronal radiation surrounding the prominence. The fine scale HeII features seen in Figure 1 can be interpreted as the optically thick surface of this prominence which surrounds the more dense features seen in  $H\alpha$ .

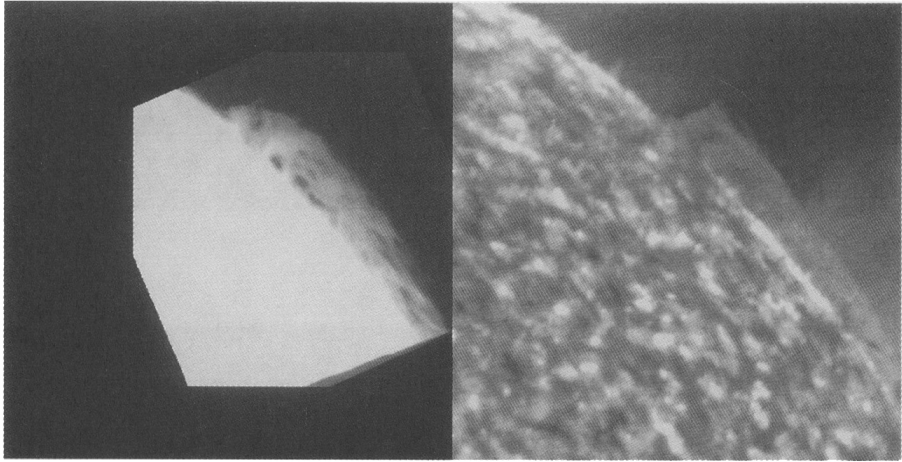
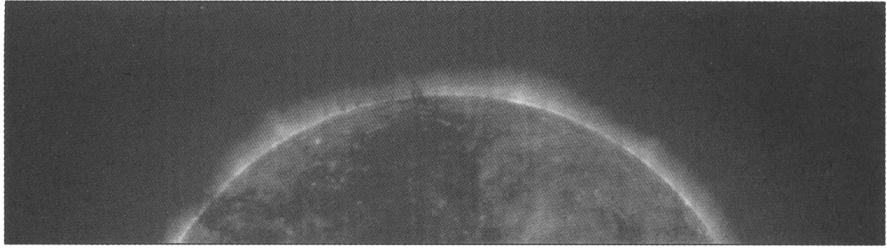


Figure 1. BBSO  $H\alpha$  (left) and EIT He II  $\lambda 304$  (right) images of a quiescent prominence on March 9, 1997 show differences in fine scale structure which can be attributed to differences in emission mechanisms. (BBSO image courtesy of H. Zirin.)

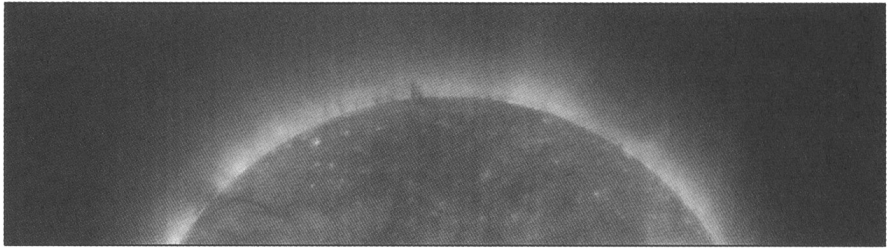
### 3. EUV Absorption Features

The observation of prominence absorption features in all the EIT passbands has been reported by Moses et al. (1997). Figure 2, the east limb on February 28, 1997, illustrates most of the characteristics of quiescent features. The figure is oriented so that solar north is to the right. To the north a prominence is seen in He II, associated with a helmet streamer structure that produces no significant absorption in the coronal lines. At the equator, a prominence aligned perpendicular to the line of sight contains absorption structures that are seen in all the coronal passbands (as well as in the He II passband). Most of the absorption structures in this prominence have the morphology of prominence feet (e.g., Tandberg-Hanssen 1995). The density, temperature, and elemental abundances in prominence feet can be expected to be quite different from those in the prominence itself. To the south is a prominence that extends onto the disk as a polar crown filament channel. In addition to the compact absorption feature seen in the coronal passbands, there is a coronal void surrounding the prominence. (This feature is a useful illustration of the amount of Si XI in the off-limb  $304 \text{ \AA}$  image.)

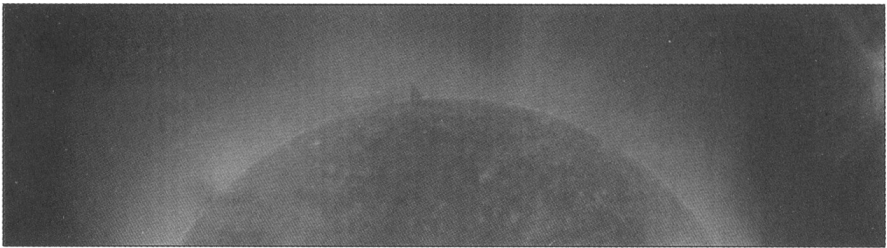
The properties of absorption features in quiescent prominences can be summarized as follows: Absorption features in the coronal passbands are visible in only part of the prominence. Prominence absorption features in the coronal passbands are less visible on the disk than the limb because, in the case of a prominence on the disk, most of the coronal material along the line of sight is between the observer and the absorbing material (particularly for the prominence feet, which extend down to the photosphere). He II prominences can exist without any detectable coronal absorption features. The absorption features in



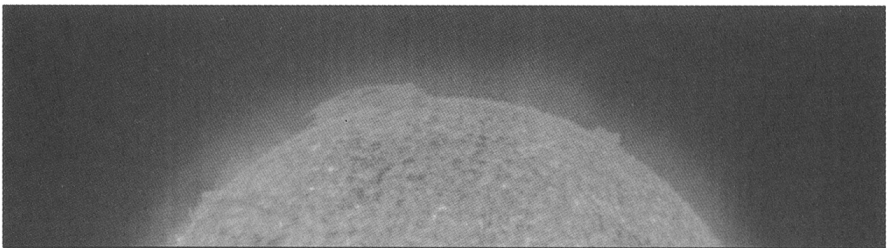
FeIX,X



FeXII



FeXV



HeII

Figure 2. February 28, 1997 image of three prominences on the east limb (solar north is to the right). The prominences at the equator and in the south can be seen as absorption features in the coronal channels.

He II are less visible than the coronal absorption features and do not necessarily match morphologically. This difference is readily appreciated as the difference between source and absorption regions in the He II and coronal images. The absorption features identified in the coronal lines are frequently below the observed surface of the He II structures in quiescent prominences (as are the H $\alpha$  emission structures described in the previous section).

An absorption feature associated with an eruptive prominence on May 31, 1997 is illustrated in Figure 3. The geometry of this configuration is particularly clear for the Fe XII absorption feature, since the absorbing material is almost entirely between the observer and the coronal emission. Collisional excitation is a much greater component of the He II emission in an eruptive prominence, so the distribution of the He II source region is different than that of quiescent prominences. Thus, the filamentary absorption region in the He II image more closely matches that in the Fe XII image. However, differences in the fine structure of the absorption feature remain, which are understood to be generated by the mixing of absorbing material and source material. (Note the shading of the He II emission at the top of the prominence, which suggests that, in this region, a significant fraction of the He II is from resonant scattering of the on-disk He II.)

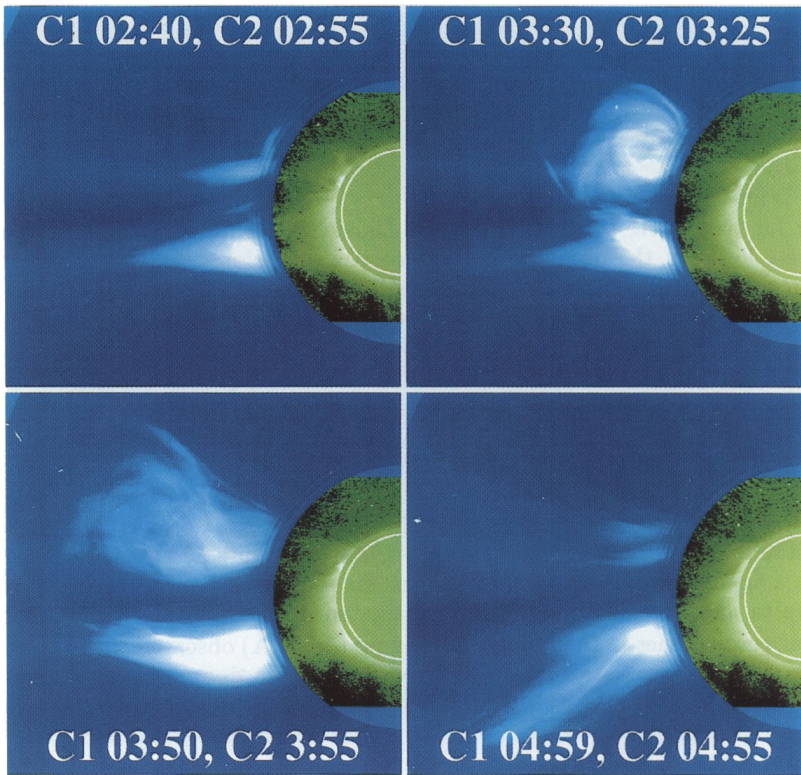
A combination of H I, He I and He II continuum absorption (Cheng, Smith, and Tandberg-Hanssen 1980, Foukal 1978, and Schmahl and Orrall 1979) constitutes a significant absorption mechanism for the EUV spectral range. Kucera, Andretta and Poland (1998) have investigated prominence absorption features in four coronal lines in the Lyman continuum ( $>504 \text{ \AA}$ ) observed with the SOHO Coronal Diagnostic Spectrometer. They found H I continuum absorption clearly sufficient to describe the total absorption in observations where the geometry of both the prominence absorption and the coronal emission is well understood. A survey by Engvold et al. (1998) of coronal absorption features in EIT images has shown that, in the absorption features readily identified in coronal images, either the continuum absorption is optically thick or other mechanisms (e.g., resonant scattering by the Fe ions) are important.

#### 4. The EIT and LASCO “CME Watch”

The great observational advance of EIT is the ability to take an extended sequence of moderate cadence (3–4 images per hour), full disk images at full resolution. Moderate cadence, full field, full resolution Fe XII image sequences, under the observational program title “CME watch”, have been the mainstay of the EIT observing program since April 1997. In the full resolution Fe XII images, the prominence absorption features trace the evolution of active prominences while the 1.5MK corona is being monitored. The transverse spatial scale of the prominence absorption features in the Fe XII images is such that a significant loss in prominence identification occurs in  $2 \times 2$  binned images ( $5.2 \times 5.2$  arcsec<sup>2</sup> pixels). The full resolution CME watch is producing an extensive range of examples of prominence evolution and of the interaction of prominences with the lower corona.

Of particular interest is the relationship of the absorption features to coronal brightenings observed during moderate cadence coronal sequences. Coronal brightenings observed on-disk along neutral lines frequently show absorption

## Large Scale Features



### Feb. 23, Coronal Mass Ejection

Figure 3. Eruptive prominence of May 31, 1997 visible as an absorption feature in Fe XII (top) and a mixture of absorption and emission in He II (bottom).

features imbedded in the coronal emission. The geometry required for such an observation implies closed field lines (for the impulsive coronal brightening) below a cooler, more dense structure (for the absorption). However, with the accumulation of many observations, examples have been observed at the limb that reveal more of the 3-dimensional configuration of coronal brightenings and require a more complicated model. The Fe XII sequence of October 9, 1997 is an example that can be viewed at <http://lasco-www.nrl.navy.mil/iau/movie.html>. During the sequence, the inner wall of the coronal cavity brightens, and then coronal emission extends across the coronal cavity. This emission crosses above and below the prominence structure seen in absorption. Viewed from above, the coronal material crossing above the filament would be more difficult to detect than the overall brightening that would be seen around the absorption feature. Thus, from a different perspective, one might interpret the observations to imply that the coronal emission was due strictly to the closing of field lines beneath

the prominence when, in reality, the situation is much more complicated. The classification and analysis of these events is an ongoing project.

The combination of LASCO and EIT observations extends the range over which the interaction between prominences and the corona can be studied from the chromosphere to the heliosphere. Skylab-era observations provided the initial breakthrough observations of prominence eruptions and CMEs (e.g., Schmahel and Hildner 1977, Poland and Munro 1976) but were restricted by the limitations of photographic film. SOLWIND and SMM coronagraph observations greatly extended the coverage of CMEs, but observations of the initiation of prominence eruptions were restricted to ground based instruments for these missions (Webb 1988).

Extended intervals of moderate cadence, full field, full resolution observations (the CME watch) have proven to be the most productive LASCO/EIT observing programs for the study of prominence eruptions and CMEs. A typical cadence for the baseline  $5.2 \text{ Kbs}^{-1}$  telemetry rate is, per hour, 3–4 EIT images (either in the FeXII or HeII passbands), 1–2 C1 FeXIV image sets, 1 C2 image and 1 C3 image. The C1 FeXIV image is obtained with a tunable Fabry-Pérot filter and requires, at the minimum, a line-center image at  $5303 \text{ \AA}$  and an off-band image at  $5309 \text{ \AA}$ .

The first CME that was well observed jointly by LASCO and EIT occurred on December 23, 1996 during the first period of high telemetry rate ( $25 \text{ Kbs}^{-1}$ ) observations (Dere et al. 1997b). The EIT observations in this sequence were made in the FeXII passband. All three components of the CME – the prominence eruption, the coronal cavity and the bright loops typical of CMEs – were present at the earliest stages observed by EIT. Observed as an FeXII absorption feature, the prominence eruption consisted of a symmetric elongation of the prominence into an upwardly expanding loop structure. The formation and acceleration of the bright loops that we interpret as the leading edge of the CME was coincident with the initiation of the prominence eruption to within the time resolution of the image cadence (12 minutes). Upon entering the C2 field of view, the CME has attained its terminal velocity of  $400 \text{ km s}^{-1}$ .

The best example of a CME sequence obtained with HeII EIT observations occurred on February 23, 1997 (Korendyke et al. 1998). The EIT HeII and C1 FeXIV observations are presented in Figure 4. As seen in FeXIV (and in the EIT coronal passbands), a large dome of coronal emission built up over the active region containing a prominence before the prominence eruption began. Over the first hour of the eruption the coronal emission slowly expanded into a shell. From the last panel of Figure 4, it can be seen that the erupting prominence material begins to fill the coronal cavity behind the expanding shell. Since the C1 coronal image is FeXIV emission, the co-spatial prominence material visible in the overlapping region of FeXIV and HeII emission must be a multi-temperature plasma with a component that is heated during the eruption to coronal temperatures ( $2 \times 10^6 \text{ K}$ ). In the last panel of Figure 4, the outer shell of the CME is just beginning to open. Following this opening of the coronal structure, acceleration occurs so rapidly that in the next image set (Figure 5), the CME has obtained its terminal velocity of  $870 \text{ km s}^{-1}$ .

The impulsive acceleration of a fast CME in the February 23, 1997 event is in marked contrast to the acceleration initiated at the beginning of the prominence

## C1 and EIT Combined Images

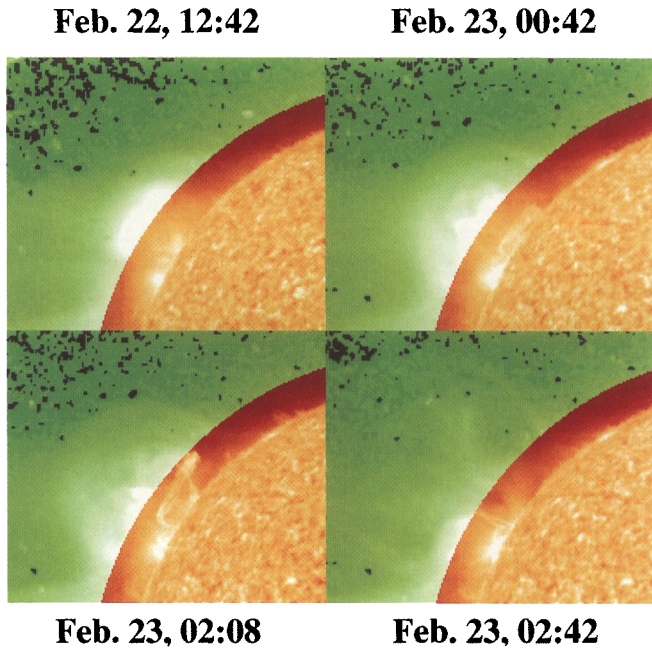


Figure 4. February 23, 1997 prominence eruption (HeII) and CME (Fe XIV) nested images illustrate the rapid heating of the chromospheric material to coronal temperatures and the sudden acceleration of the CME front.

eruption in the December 23, 1996 slow CME event. In both events, the CME had reached its terminal velocity upon entering the C2 field of view. Although the prominence velocity was approximately the same for both events, the twist and general complexity was much greater in the eruptive prominence associated with the fast CME. The large-scale evolution of the fast CME on February 23 is seen in Figure 5. The evolution observed in the C1 and EIT images is not apparent in the larger scale C2 images. In the later phase of the CME, as seen in the C2 images, the prominence eruption appears to be located in one leg of the overall CME, suggesting that the pre-existing coronal field configuration was complex (e.g., Webb 1998, these proceedings).

From the fast CME sequence of February 23, 1997, it is clear that the prominence eruption does not drive the CME. Although the prominence eruption and CME are associated, the acceleration of the CME is poorly matched to the evolution of the prominence. The event appears very different in each of the three instruments, demonstrating the observational advances achieved through the combination of the capabilities of EIT and LASCO. This new capability of imaging the corona below  $1.5 R_{\odot}$  with good temporal resolution provided by the LASCO C1 and EIT combination greatly extends our understanding of the initiation of CMEs.

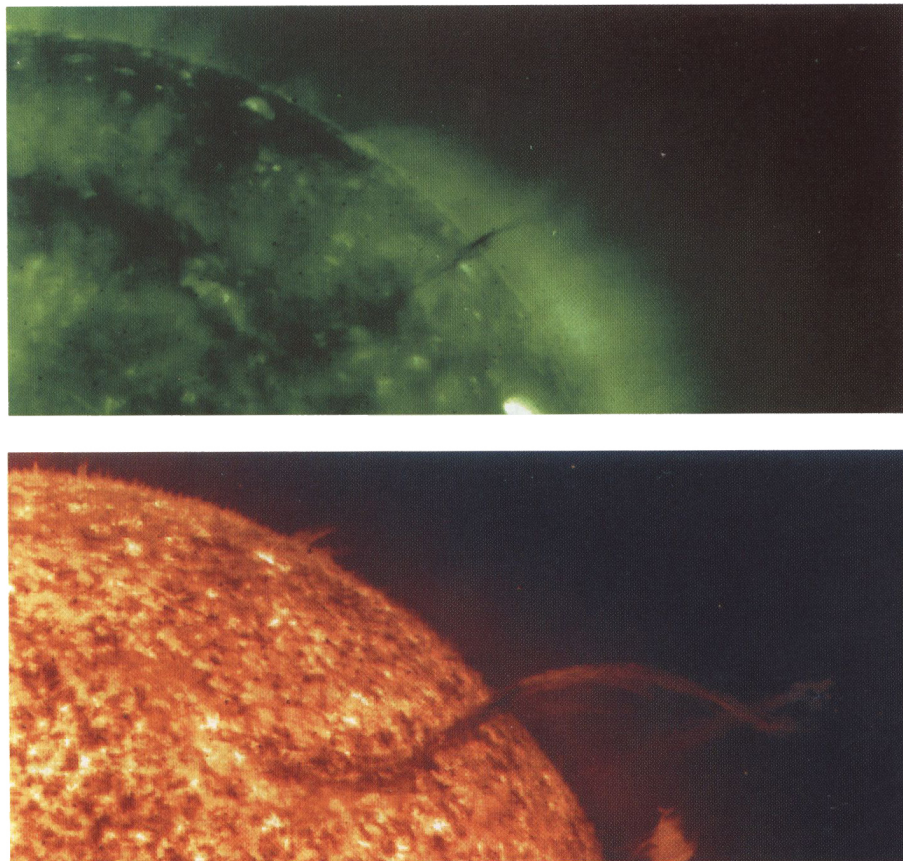


Figure 5. February 23, 1997 CME composite of Fe XIV (C1) and continuum (C2) images illustrates the evolution of the event.

**Acknowledgments.** We are very grateful to the dedicated LASCO and EIT operations teams. The authors received support from the Office of Naval Research and NASA grants NDPRS-86759E and NDPRS-09930F. Helpful comments were contributed by V. Andretta, J.W. Cook, O. Engvold, H. Jakobsson, T. Kucera, M. Laming, K. Waljeski, K. Widing, and H. Zirin. J. Newmark and R. Duffin helped with the figures. The combined LASCO and EIT consortium members are G. Brueckner, J.W. Cook, K. Dere, R. Howard, M. Koomen, C. Korendyke, R. Kreplin, D. Michels, D. Moses, N. Moulton, D. Socker, C. St.Cyr, J.P. Delaboudinière, C. Jamar, J.M. Defise, P. Rochus, R. Catura, J. Lemen, J. Gurman, J. Newmark, B. Thompson, W. Neupert, F. Clette, P. Cugnion, P. Lamy, A. Llebaria, R. Schwenn, and G. Simnett.

**References**

- Cheng, C.C., Smith, J.B., and Tandberg-Hanssen, E. 1980, *Solar Phys.*, 45, 393
- Delaboudinière, J.-P. et al. 1995, *Solar Phys.*, 162, 291
- Dere, K.P., Landi, E., Mason, H.E., Monsignori Fossi, B.C., and Young, P.R. 1997a, *A&A*, 125, 149
- Dere, K.P. et al. 1997b, *Solar Phys.*, 175, 601
- Dere, K.P. and Mason, H.E. 1993, *Solar Phys.*, 144, 217
- Engvold, O., Jakobsson, H., Tandberg-Hanssen, E., Harvey, K.L., Moses, D., and Gurman, J.B. 1998, in preparation
- Foukal, P. 1978, *ApJ*, 223, 1046
- Jordan, C. 1975, *MNRAS*, 170, 429
- Jordan, S.D., Thompson, W.T., Thomas, R.J., Neupert, W.M. 1993, *ApJ*, 406, 346
- Korendyke, C.M. et al. 1998, in preparation
- Kucera, T.A., Andretta, V., and Poland, A.I. 1998, in preparation
- Laming, J.M. and Feldman, U. 1992, *ApJ*, 386, 364
- Laming, J.M. and Feldman, U. 1993, *ApJ*, 403, 434
- Moses, D. et al. 1997, *Solar Phys.*, 175, 571
- Poland, A.I. and Munro, R.H. 1976, *ApJ*, 209, 927
- Schmahl, E.J. and Hildner, E. 1977, *Solar Phys.*, 55, 473
- Schmahl, E.J. and Orrall, F.Q. 1979, *ApJ*, 231, L41
- Tandberg-Hanssen 1995, *The Nature of Solar Prominences*, Kluwer Acad. Publ., Dordrecht, Holland
- Thomas, R. 1994, *EOS*, 16, 269
- Tousey, R., Bartoe, J.D.F., Brueckner, G.E., Purcell, J.D. 1977, *Appl. Optics*, 16, 870
- Webb, D.W. 1988, *J. Geophys. Res.*, 93, 1749
- Zirin, H. 1975, *ApJ*, 199, L63